ADVANCED MATERIALS

Supporting Information

for *Adv. Mater.,* DOI: 10.1002/adma.202210828

Room-Temperature Magnetism in 2D $MnGa_4$-H Induced by Hydrogen Insertion

Nan Wei, Liangcheng He, Changwei Wu, Dabiao Lu, Ruohan Li, Haiwen Shi, Haihui Lan, Yao Wen, Jun He, Youwen Long, Xiao Wang,* Mengqi Zeng,* and Lei Fu**

Supporting Information

Room-Temperature Magnetism in Two-Dimensional $MnGa_4$-H Induced by Hydrogen Insertion

Nan Wei[#], Liangcheng He[#], Changwei Wu[#], Dabiao Lu, Ruohan Li, Haiwen Shi, Haihui Lan, Yao Wen, Jun He, Youwen Long, Xiao Wang*, Mengqi Zeng*, and Lei Fu**

[#] *These authors contributed equally to this work.*

Figure S1. Schematic illustration of the growth process of bulk $MnGa_4$. The energy barrier for lateral motion is relatively high on Ga_2O_3/Ga surface due to the strong interaction between Ga_2O_3 and Ga, which could seriously limit the lateral diffusion rate of precursor Mn atoms, leading to a three-dimensional island growth mode of $MnGa_4$.

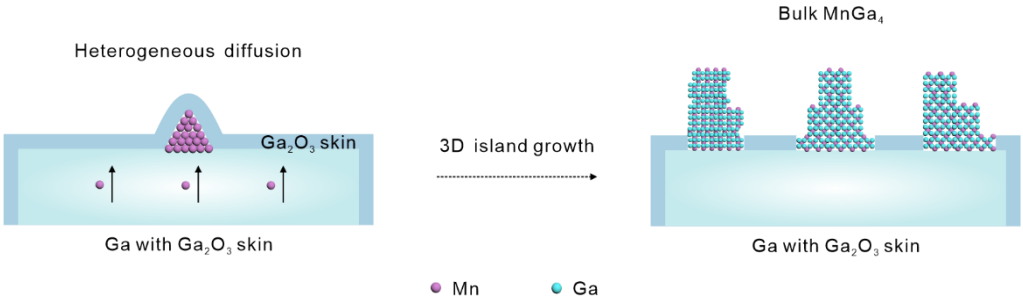

Figure S2. Energy dispersive X-ray spectroscopy (EDS) measurement for pristine Ga surface and H_2-plasma treated Ga surface. The acceleration voltage of the electron beam is 8 kV. a) EDX spectra and oxygen atom weight percentage of pristine Ga surface. b) EDX spectra and oxygen atom weight percentage of H_2-plasma treated Ga surface. After the H_2-plasma treatment, the oxygen content of the gallium surface is significantly reduced, and the surface is quite flat and smooth.

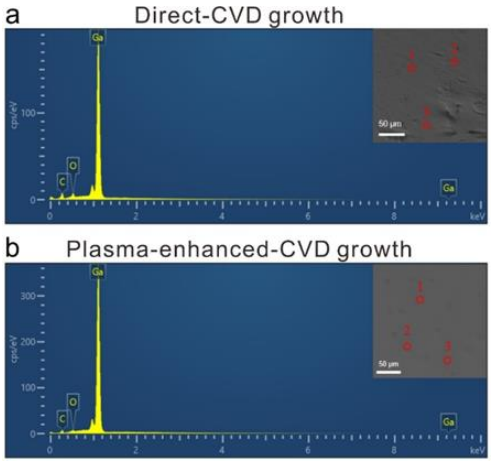

	O (wt%)
1	1.45
2	1.63
3	1.19
average	1.42

	O (wt%)
1	0.54
2	0.51
3	0.52
average	0.52

Figure S3. OM images of Ga surface adopt the direct-CVD growth route and H_2-plasma treated CVD growth route.

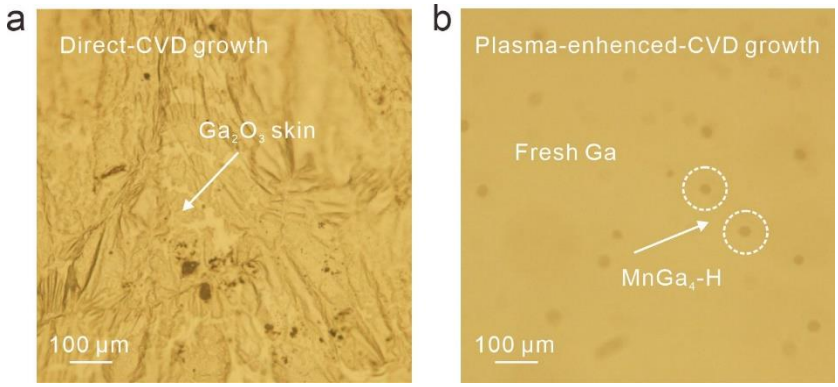

Figure S4. SEM images of the Ga surface adopt the direct-CVD growth route and the H_2-plasma-treated CVD growth route.

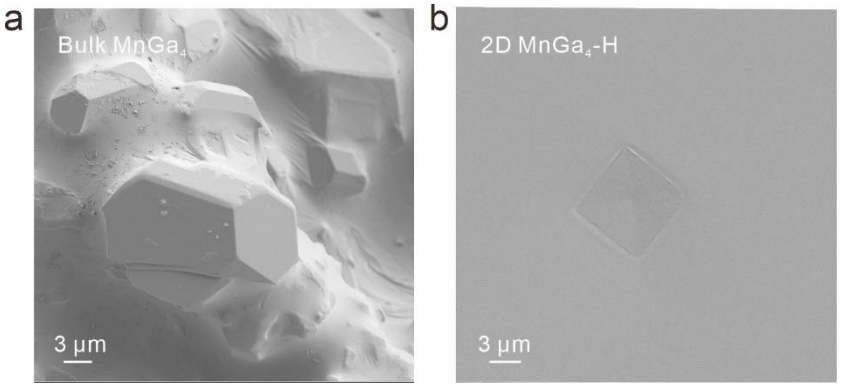

Figure S5. The XRD θ-2θ pattern of the bulk $MnGa_4$ samples grown without plasma treatment. It is corresponding well to the reported cubic $MnGa_4$ (*Im*-3*m*, No. 229) with lattice parameter a = 5.5961(6) Å, V = 175.06(2) $Å^3$ and Z = 2, indicating that pure $MnGa_4$ phase was synthesized. The substrate is a conductive tape, which was used to load the bulk $MnGa_4$, and its XRD pattern is also shown in this figure.

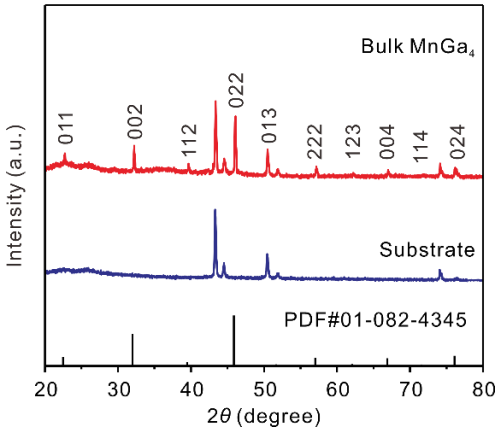

Figure S6. The XRD θ-2θ pattern of W substrate. the XRD pattern of our W substrate is well matched to the body-centered cubic (bcc) phase of the α-W pattern (PDF#004-0806).

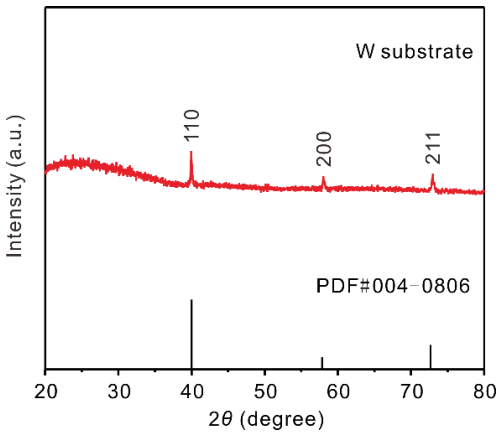

Figure S7. XRD θ-2θ patterns of 2D $MnGa_4$-H on W substrates at different treatment times. a) Comparison of XRD spectra of 2D $MnGa_4$-H intermediates collected at different H_2-plasma treatment times. b) Lattice parameter change measured from corresponding XRD (a). The measured XRD peaks shifted to lower angles during the H_2-plasma-assisted reaction, indicating the expanded crystal lattices. The sharp XRD diffraction patterns further verify the high crystallization quality of 2D samples. The crystal lattices of the products obtained at 120 min to 150 min are similar, indicating that the growth process of $MnGa_4$-H is completed at 120 min. The lattice parameter of 2.97 Å obtained at 120 min matches well with 2.93 Å measured by HAADF-STEM shown in Fig. 2.

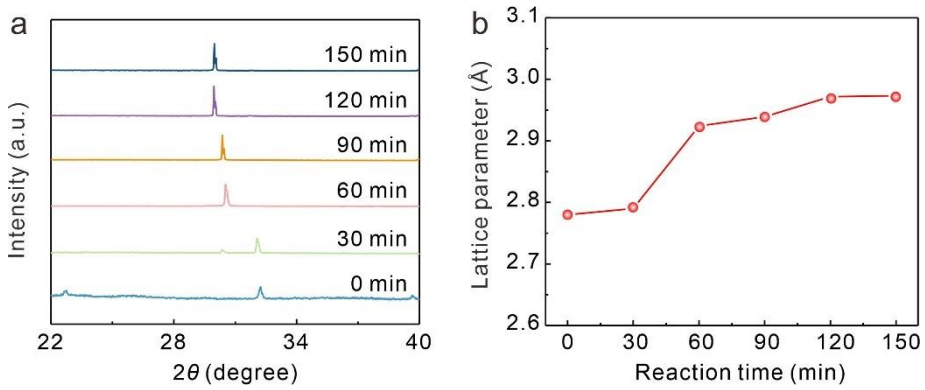

Figure S8. XRD θ-2θ patterns of 2D $MnGa_4$-H on W substrates at different annealing temperatures compared to the sample kept at room temperature.

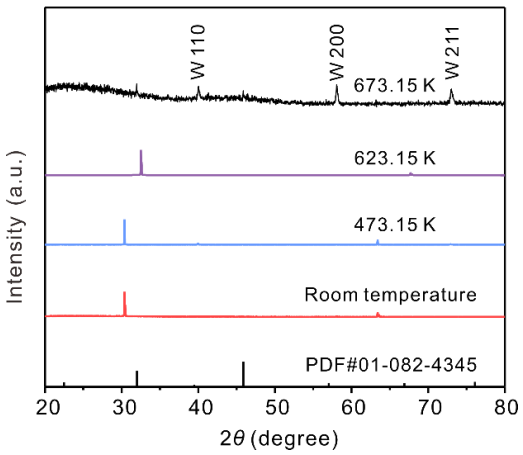

Figure S9. ToF-SIMS analysis of 2D $MnGa_4$-H on W substrates. a) Normalized ToF-SIMS depth profile of hydrogen ions for 2D $MnGa_4$-H before and after dehydrogenation. b) Cross-section ToF-SIMS secondary mapping of hydrogen ions for 2D $MnGa_4$-H. c) Cross-section ToF-SIMS secondary mapping of hydrogen ions after dehydrogenation. We conduct dehydrogenation by annealing the sample at 623.15 K for one hour under the vacuum condition. We use negative ion mode to detect the presence of hydrogen. After high-temperature annealing, the hydrogen content can be observed to decrease in-depth profile (a). The position of the interface is judged by the time when the hydrogen content starts to stabilize, hydrogen signal can be observed at the top of cross-section ToF-SIMS secondary mapping (b), which is also the area where the single crystal is located. Below the single crystal is the signal of the substrate. After annealing, there is almost no hydrogen signal in the whole area (c).

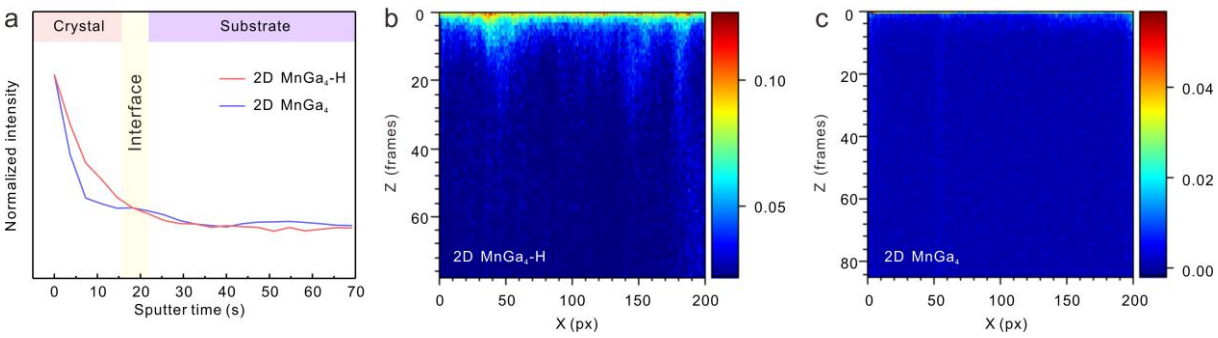

Figure S10. The XRD θ-2θ patterns of the bulk $MnGa_4$ samples grown with H_2-plasma and treated by H_2-plasma. The substrate is a conductive tape, which was used to load the bulk $MnGa_4$, and its XRD pattern is shown in this figure. The peaks of the two samples did not shift, indicating that the bulk sample did not undergo lattice expansion after H_2 plasma treatment under the same conditions as 2D $MnGa_4$. This may be because the activity of the H atoms at this power is not sufficient to permeate the entire bulk samples compared with 2D samples. On the other hand, the thicker passivation layer (composed of oxides, water, hydroxides, and carbon oxides) on the surface of the bulk samples could prevent the chemical dissociation and adsorption of H on the gas-solid surface and the penetration of hydrogen atoms on the surface.[1]

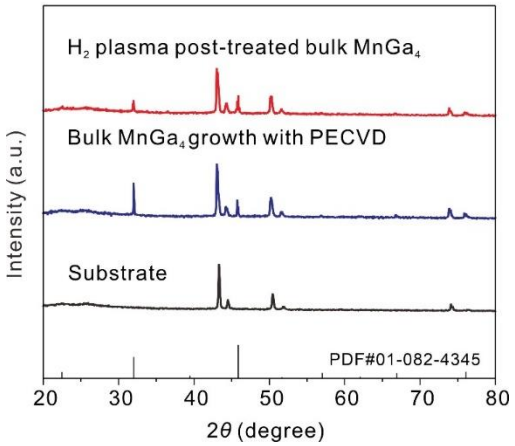

Figure S11. The high-resolution deconvoluted Ga 2p XPS spectra of the bulk $MnGa_4$ and 2D $MnGa_4$-H. The Ga 2p peaks of the 2D $MnGa_4$-H shift to lower binding energy compared with the bulk $MnGa_4$. This proves that there is charge transfer between them, thereby leading to Ga with electron-deficient status in the $MnGa_4$-H. This modification of electronic structures indirectly proves the insertion of hydrogen atoms.

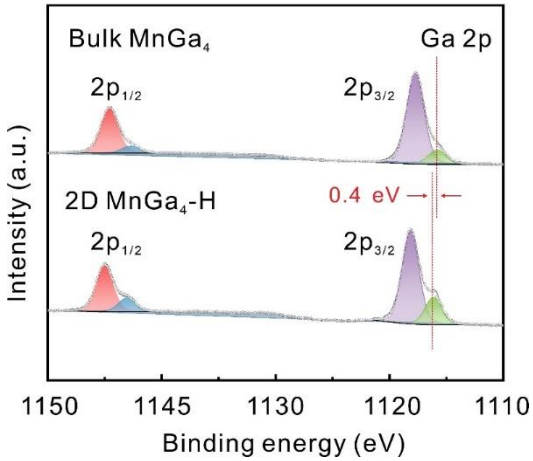

Figure S12. The high-resolution O 1s XPS spectra of the (a) bulk $MnGa_4$ and (b) 2D $MnGa_4$-H. The unavoidable surface oxidation of the intermetallic phase is a common phenomenon and is often observed in intermetallic compounds. For bulk samples (a), The surface oxidation was confirmed from O 1s XPS spectra where two deconvoluted peaks (I and II) at 531.0 eV and 532.5 eV can directly be ascribed to surface hydroxylation and surface-adsorbed oxygen species. For 2D samples (b), The O 1s XPS spectra could be deconvoluted into four peaks (I, II, III, and IV)) where the peak at 529.7 eV is due to the formation of oxide species while the peaks at 531.1, 532.3, and 533.7 eV can be attributed to surface hydroxylation,[2] surface-adsorbed oxygen species, and water adsorbed onto the surface.[3] The difference in peaks between bulk and 2D samples may be due to the oxidation and adsorption caused by the contact of 2D samples with water during the transfer process.

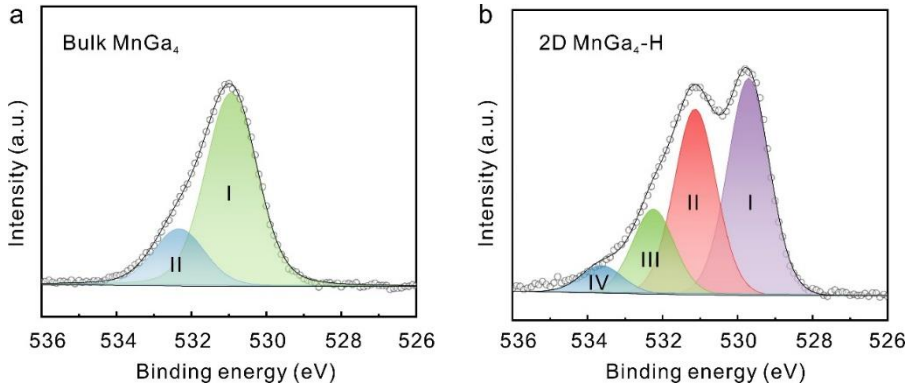

Figure S13. Environmental stability investigations. a–d) Optical images of 2D $MnGa_4$-H samples exposed in the atmosphere for 0 day, 7 days, 14 days, and 21 days, respectively. After exposure to air for 7 days, the color and morphology of the sample remained unchanged, which was equivalent to that of the fresh sample. When the exposure time was extended to more than 14 days, the edge of the sample began to slightly deteriorate. Finally, after exposure to air for 21 days, the surface of the sample was rugged and completely degraded.

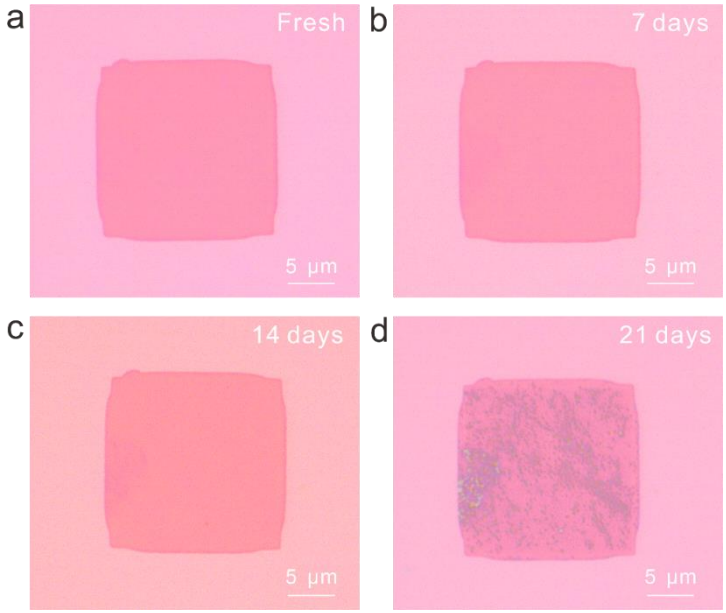

Figure S14. The evolution of XRD θ-2θ patterns over time. The intensity is in logarithmic scale. * indicates the XRD peaks of the surface oxidation. It can be seen that the XRD pattern basically remains unchanged after exposure to air for 7 days, indicating good air stability. When the exposure time was extended to 14 days, the impurity peaks begin to appear and the composition of the sample is no longer single. This may be due to surface oxidation when exposed to air.

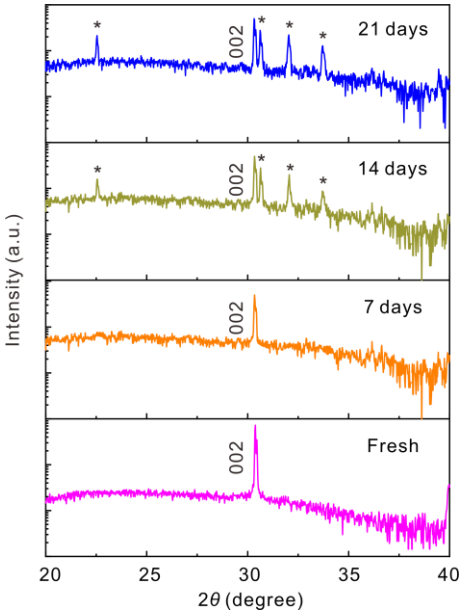

Figure S15. Schematic of the metal foil-assisted etching-free transfer process. W foil was employed as a transfer medium for sample transfer due to its stable chemical properties, high hardness, and no reaction with air/water at room temperature. We put the W foil on the liquid Ga surface. The sample will be separated from the surface of Ga oxidized by air due to the strong affinity between metals[4]. Residual Ga on the surface of W foil can be easily removed after ultrasonic in water. It is worth noting that this transfer process can be completed in a few seconds, which is much faster than the traditional methods, and the morphology of transferred samples is reserved perfectly.

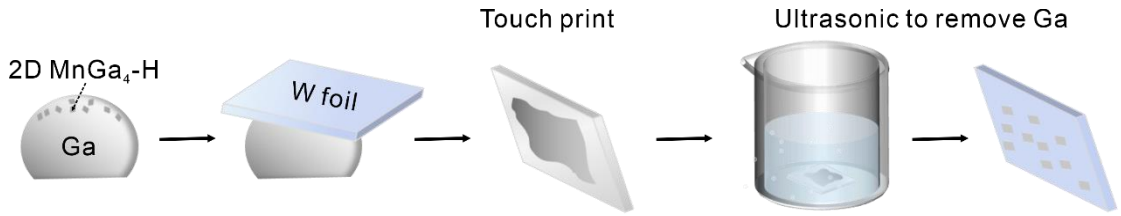

Figure S16. The EDX spectrum of the 2D $MnGa_4$-H single crystal. The peaks for Cu can be correlated to the TEM grid (carbon film on 300 mesh Cu-grid).

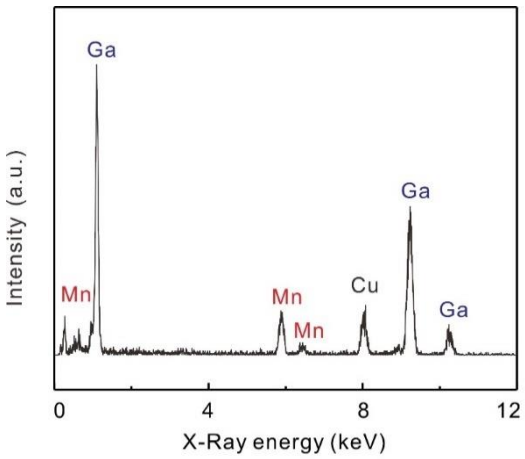

Figure S17. The selected-area electron diffraction (SAED) of 2D $MnGa_4$-H crystal. Only one set of tetragonal diffraction spots exists confirming the excellent single-crystal nature of the 2D $MnGa_4$-H.

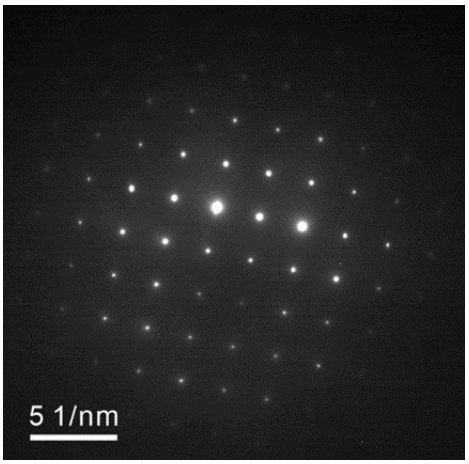

Figure S18. *M–H* curves of the growth substrate (W foil) at different temperatures. The linear *M–H* curves with zero hysteretic loops taken at different temperatures indicate a paramagnetic background of W substrate.

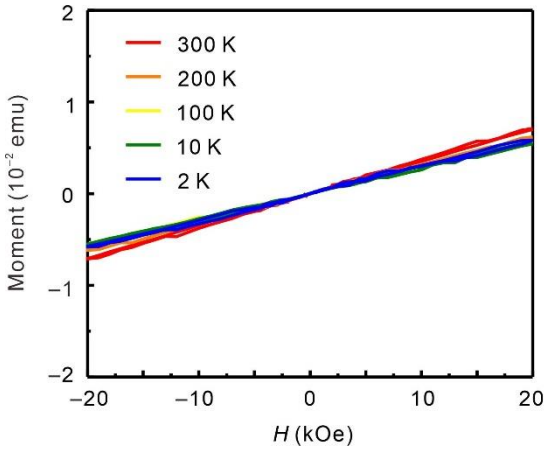

Figure S19. Magnetic properties of bulk $MnGa_4$. a) The temperature dependence of the *M–T* curve of bulk $MnGa_4$ measured in the H = 1 kOe from 300 to 600 K. b) *M–H* curve of bulk $MnGa_4$ at 300 K with magnetic field ranging from −20 to 20 kOe. The inset shows the *M–H* curves on a narrow scale for better perception.

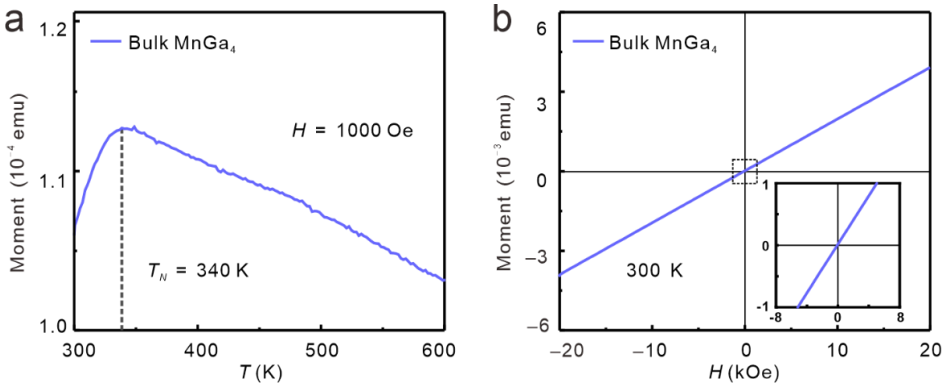

Figure S20. The *M–H* curve of 2D $MnGa_4$-H after dehydrogenation at 300 K, showing a nonmagnetic response. We conduct dehydrogenation by annealing the sample at 623.15 K for one hour under the vacuum condition.

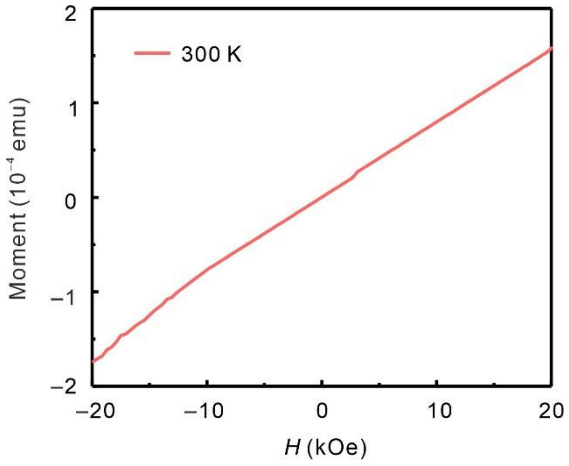

Figure S21. *M–H* curves of 2D $MnGa_4$-H at different H_2 plasma exposure time on a narrow scale around 0 Oe. From (a–e), the exposure time increased from 0 min to 120 min.

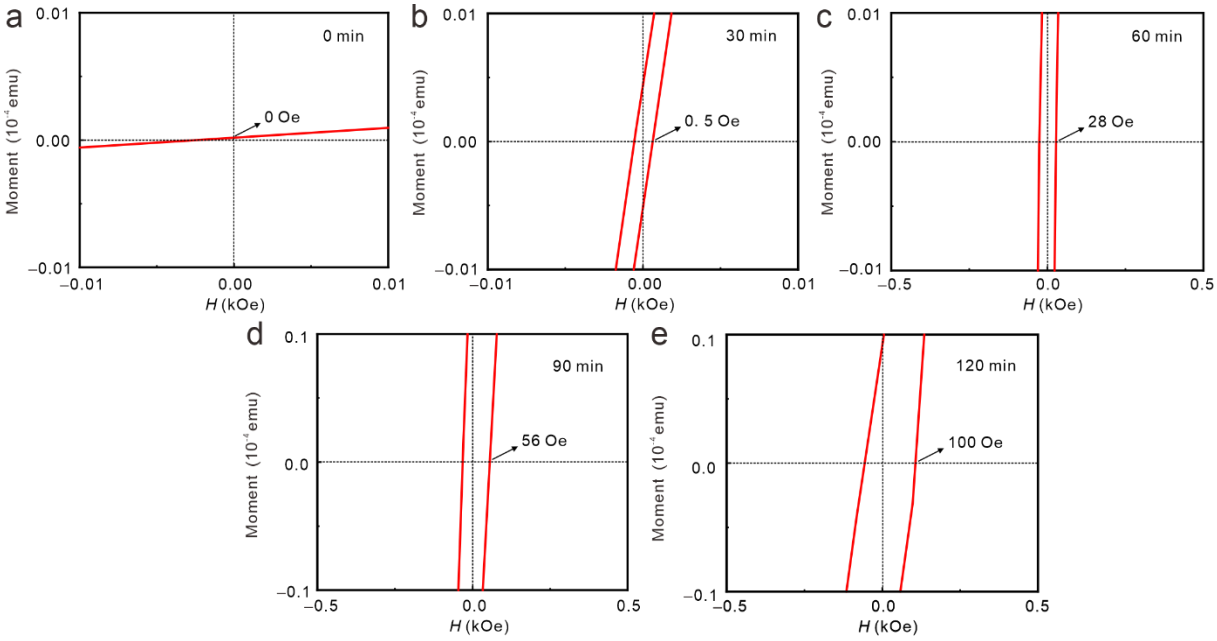

Figure S22. Magnetic anisotropy of 2D $MnGa_4$-H single crystals, showing an out-of-plane easy magnetization axis.

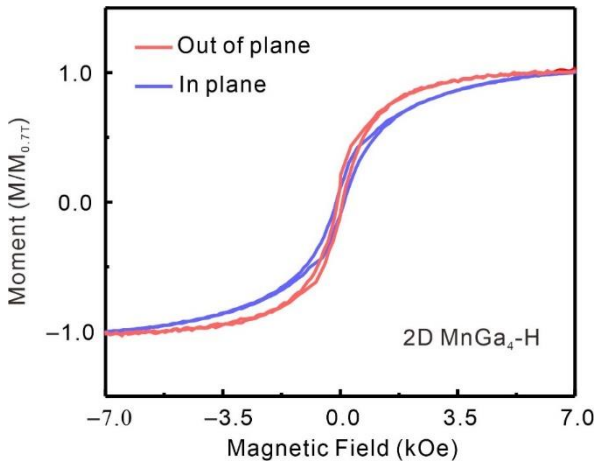

Figure S23. Height profile of 2D $MnGa_4$-H. a) The corresponding height profile of the as-fabricated Hall bar device with a thickness of 5.5 nm. b) The corresponding height profile of the as-fabricated Hall bar device with a thickness of 19.0 nm.

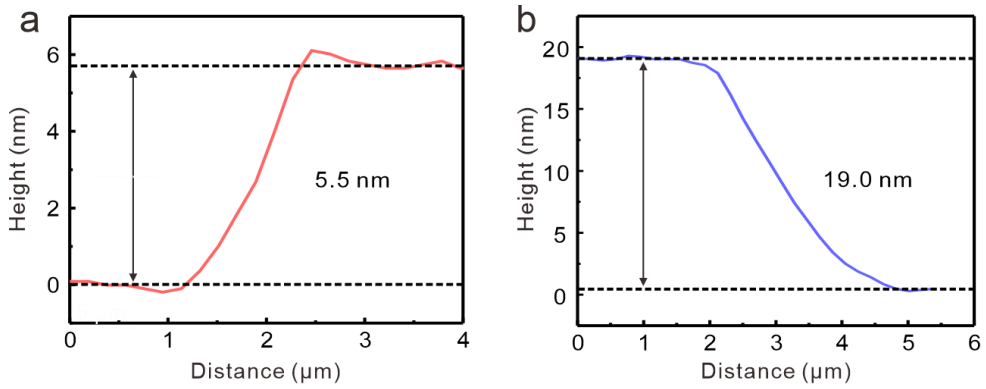

Figure S24. Hydrogen migration barriers in bulk $MnGa_4$ and 2D $MnGa_4$. It indicates that hydrogen has a lower migration barrier in 2D $MnGa_4$ and it is easier to insert hydrogen in 2D $MnGa_4$.

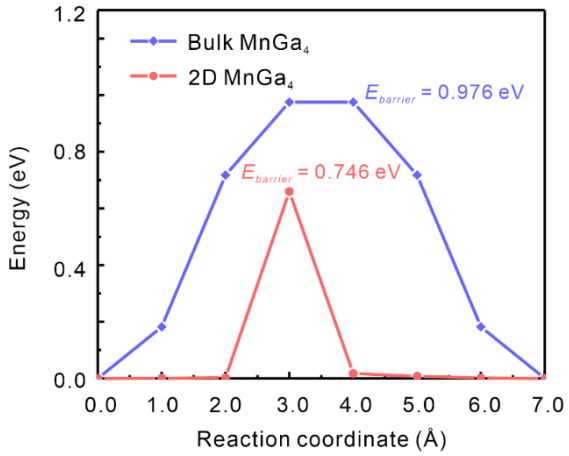

Figure S25. Schematic and geometry of four-probe devices for resistance measurement.

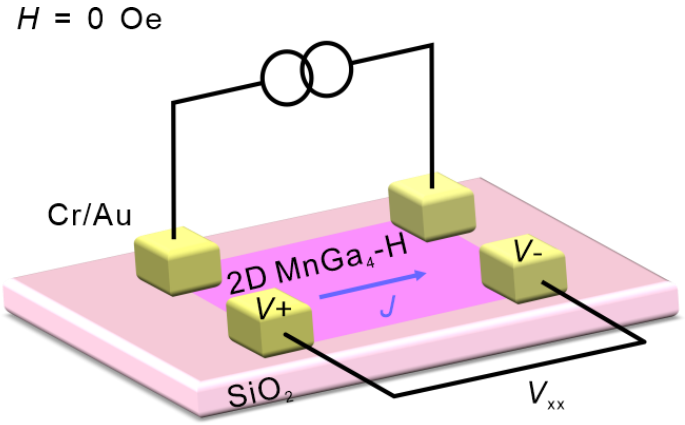

Figure S26. The adsorption energy of hydrogen at different sites in 2D $MnGa_4$. It shows that hydrogen adsorption at the center of the face is the most stable.

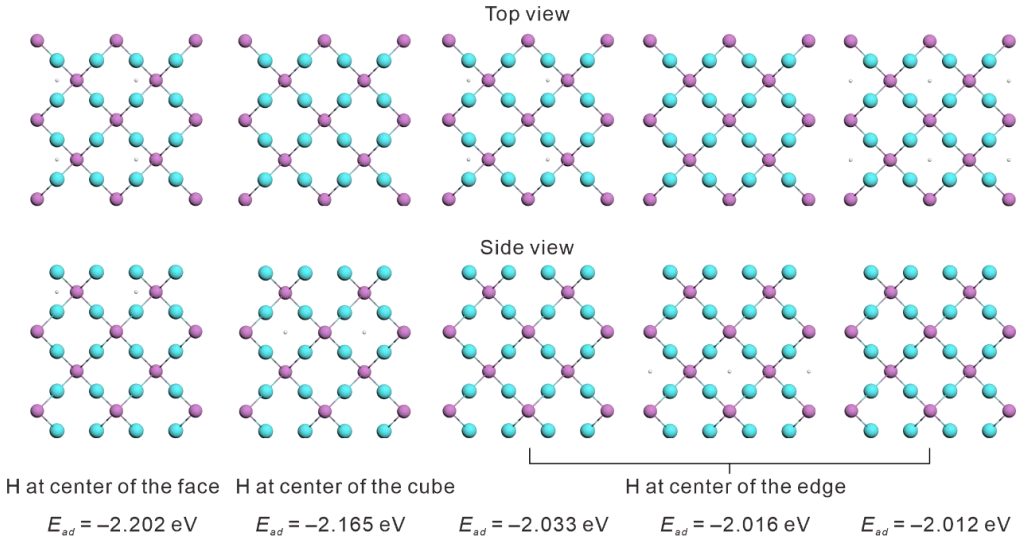

Figure S27. Molecular dynamics simulation of hydrogen at different adsorption sites. When hydrogen is adsorbed at the center of the face, the framework of the structure is well maintained after simulation, which verifies the conclusion that the center of the face is the optimal adsorption site.

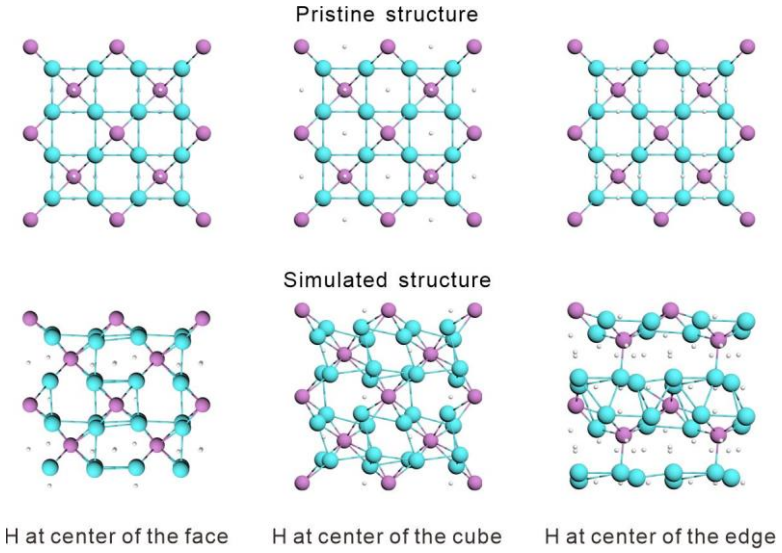

Figure S28. The calculated atomic magnetic moments of 2D $MnGa_4$-H with different amount of H incorporation.

a

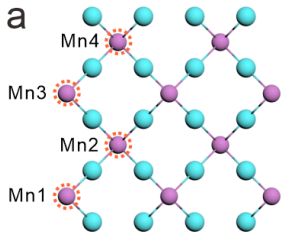

atom	Magnetic moment (μ_B)
Mn1	1.32
Mn2	-1.45
Mn3	1.44
Mn4	-1.38

b

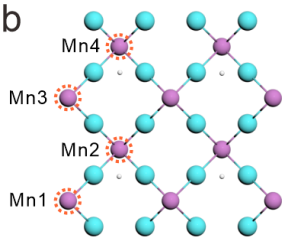

atom	Magnetic moment (μ_B)
Mn1	1.51
Mn2	-0.97
Mn3	1.53
Mn4	-0.86

c

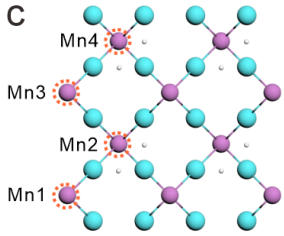

atom	Magnetic moment (μ_B)
Mn1	1.58
Mn2	-0.24
Mn3	1.82
Mn4	-0.05

d

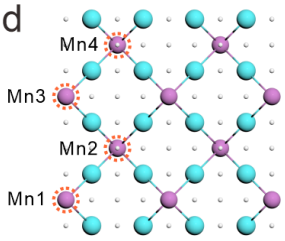

atom	Magnetic moment (μ_B)
Mn1	2.58
Mn2	-0.01
Mn3	2.66
Mn4	-0.09

Figure S29. The calculated exchange energy Δ*E* (eV) variation with the degree of hydrogen insertion. It can be seen that the exchange energy increases as the degree of hydrogen insertion increases, indicating that the gradual transition process from antiferromagnetic state to ferrimagnetic state.

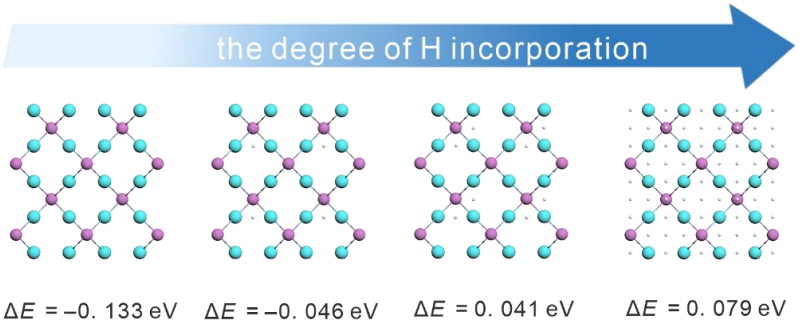

Table S1. Air stability of reported 2D metals.

No.	Sample	Air stability	Ref.
This work	**2D $MnGa_4$-H single crystals**	**7 days**	**This work**
1	2D Ga, In and Sn single crystals	Can not exist in the air without graphene encapsulation	*Nat. Mater.* **2020**, *19*, 637
2	2D Fe membranes	Can not exist in the air without graphene encapsulation	*Science* **2014**, *343*, 1228
3	2D Cr membranes	Can not exist in the air without graphene encapsulation	*Nano Lett.* **2020**, *20*, 4354
4	2D Co layers	Oxidize rapidly in the air	*Nature* **2016**, *529*, 68
5	2D Ga films	Oxidize rapidly in the air	*Sci. adv.* **2018**, *4*, e1701373
6	2D Fe nanoflakes	6 days	*Matter* **2022**, *5*, 291

References

[1] J. Bloch, M. H. Mintz, *J. Alloys Compd.* **1997**, *253-254*, 529.

[2] X. Chen, L. Liu, P. Y. Yu, S. S. Mao, *Science* **2011**, *331*, 746.

[3] W. Hu, Y. Liu, R. L. Withers, T. J. Frankcombe, L. Noren, A. Snashall, M. Kitchin, P. Smith, B. Gong, H. Chen, J. Schiemer, F. Brink, J. Wong-Leung, *Nat. Mater.* **2013**, *12*, 821.

[4] K. Le Vay, B. M. Carter, D. W. Watkins, T. Y. Dora Tang, V. P. Ting, H. Colfen, R. P. Rambo, A. J. Smith, J. L. Ross Anderson, A. W. Perriman, *J. Am. Chem. Soc.* **2020**, *142*, 20640.